

Supporting Information

A reversed gas diffusion electrode enables collection of high purity gas products from CO₂ electroreduction

Bo Wu^{1,2,8}, Lakshmi Devi Voleti^{1,8}, Aidan Q. Fenwick^{3,4}, Chao Wu⁵, Jiguang Zhang^{1,2}, Ning Ling¹, Meng Wang^{1,2}, Yuewen Jia¹, Weng Weei Tjiu², Mingsheng Zhang², Zainul Aabdin², Shibo Xi⁵, Channamallikarjun S. Mathpati⁶, Sui Zhang¹, Harry A. Atwater^{3,7}, Iftekhhar A. Karimi¹ and Yanwei Lum^{1,2*}

¹Department of Chemical and Biomolecular Engineering, National University of Singapore, Singapore.

²Institute of Materials Research and Engineering, Agency for Science, Technology and Research, Singapore.

³Liquid Sunlight Alliance, California Institute of Technology, Pasadena, California, United States of America.

⁴Department of Chemistry and Chemical Engineering, California Institute of Technology, Pasadena, California, United States of America.

⁵Institute of Sustainability for Chemical, Energy and Environment, Agency for Science, Technology and Research, Singapore.

⁶Department of Chemical Engineering, Institute of Chemical Technology, Matunga, Mumbai, India.

⁷Department of Applied Physics and Materials Science, California Institute of Technology, Pasadena, California, United States of America.

⁸These authors contributed equally to this work.

*Corresponding author: lumyw@nus.edu.sg

Methods

Materials. Potassium carbonate (99.995%) were purchased from Sigma-Aldrich. The porous hydrophobic polytetrafluoroethylene (PTFE) substrates with different pores size were purchased from Beijing Zhongxingweiye Instrument Co., Ltd. Deionized water (18.2 M Ω) from an OmniaPure UltraPure Water System (Stakpure GmbH) was used for all the experiments. The Au (99.999%), and Ag (99.999%) targets were obtained from Kurt J. Lesker Company. Carbon dioxide (99.9%) and oxygen (99.9%) were obtained from Air Liquide Singapore Pte. Ltd. The flow cell was purchased from Gaosunion Co., Ltd. The standard calibration gas mixtures for calibrating the gas chromatography system were obtained from Air Liquide Singapore Pte. Ltd. All the chemicals used in this work were of analytical grade and used without further purification.

Preparation of Au/PTFE(X) and NP Au/PTFE. Au/PTFE was prepared by depositing 200, 300 or 500 nm of Au onto porous hydrophobic PTFE substrates using a magnetron sputtering system (Cello Ohmiker-30CSL). The thickness of the Au can be controlled by simply adjusting the sputtering duration. NP Au/PTFE was prepared by first depositing AuAg alloys followed by subsequent dealloying¹. Firstly, AuAg alloys of 300 nm thickness were coated onto the hydrophobic PTFE membrane using an AMOD dual electron beam deposition system (System 02520, Angstrom Engineering). To adjust the Au and Ag composition, the deposition rates were adjusted as required. The ratios of the Au and Ag for these catalysts are 1:9, 1:4 and 3:7, which was analyzed by X-ray photoelectron spectroscopy (XPS). After that, the nanoporous Au was derived by etching the AuAg alloys in concentrated HNO₃. The PTFE membrane coated with the AuAg alloy was placed onto a plate and concentrated HNO₃ was dripped onto the catalyst surface. After 5 min, the color of the catalyst changes from grey to brown, which indicates that the etching process was complete. Following this, the catalyst was washed with DI water and dried in an oven for 12 h.

Characterization. The morphology and microstructure of the samples were characterized by field emission scanning electron microscopy (FE-SEM, Hitachi S-4800, 3-5 kV) and transmission electron microscopy (TEM, JEOL JEM-2100F, 200 kV). XPS of the samples were carried out on a Physical Electronics PHI 1600 ECSA system with an Al Ka X-ray source ($E=1486.6$ eV). The binding energy was calibrated against the C 1s photoelectron peak at 284.6 eV as the reference. X-Ray powder diffraction (XRD) measurements were performed on a Bruker D8 Discover 3 diffractometer with Cu $K\alpha$ radiation under 40 kV and 40 mA.

Wettability test. Wettability tests were conducted on a drop shape analysis system with a sessile drop method applied by a contact angle tester (Shanghai Zhongchen Digital Technology Apparatus Co., Ltd., Powereach JC2000C1) under ambient conditions at room temperature. The spreading of the water droplet with a volume of 0.45 μL on the sample surface over time was observed, while the wettability of the samples was estimated by observing the contact angle of the water droplet on the surface at the stable state.

Gas permeation tests. The pure gas (H_2 and CO_2) permeance of membranes was measured using a variable-pressure constant-volume gas permeation cell. Before the tests, the membranes were vacuumed overnight in the cell. The tests were performed at different trans-membrane pressures under a temperature of 30 $^\circ\text{C}$ with different gas applied. Three samples were tested for each gas and the average was reported with a standard deviation of <10%. The gas permeance can be calculated according to the Equation:

$$P_i = \frac{V_{STP}}{A \times \Delta P \times t}$$

(4) where P_i is the membrane permeance of a gas in GPU (1 GPU = 1×10^{-6} $\text{cm}^3_{\text{STP}} \text{cm}^{-2}\text{s}^{-1}\text{cmHg}^{-1}$), V is the volumetric flow rate at standard temperature pressure (cm^3), A is the effective membrane area (cm^2), ΔP is the gas pressure difference across the membrane.

Electrochemical measurements. CO_2R experiments were conducted in a flow cell, with different Au as the cathode catalyst. Electrochemical measurements in this work were carried

out using an Autolab PGSTAT204. The reported current densities are based on the geometric surface area of 1 cm². During the measurement, CO₂ was purged into the catholyte while small CO₂ bubbles also flowed with the catholyte into the catholyte chamber. N₂ gas was passed through the cathode gas chamber at a flow rate of 30 sccm using a mass flow controller (Alicat Scientific). As for electrolysis with CO₂ feedstock containing O₂ impurities, a mixture of O₂ and CO₂ was used in which the mass flow of each gas was controlled by a mass flow controller.

Bicarbonate electrolysis. The two-electrode system was employed to investigate the performance of bicarbonate electrolysis. Specifically, a membrane electrode assembly (MEA), is consisted of a nanoporous Au/PTFE(0.45) cathode, a Ni foam anode, and a bipolar membrane. 3 M KHCO₃ solution and 1 M KOH were fed as the catholyte and anolyte, respectively. The headspace of the outer electrolyte reservoir was collected and tested by the gas chromatography mass spectrometry (GCMS).

Product analysis and quantification. CO₂ reduction gas products were analyzed using an Agilent 8600 gas chromatography (GC) system equipped with a thermal conductivity detector and a flame ionization detector. The equation used for calculating the gas product FE is:

$$FE = \frac{N \times v \times c \times F}{i \times V_m}$$

Where N is the electron transfer number, v is the gas flow rate, c is the concentration of the detected gas product, F is the Faraday constant, i is the total current and V_m is the unit molar volume of gas. The outlet gas flow rate of the electrochemical cell was measured using a bubble flow meter.

The GC-MS product was tested in An Agilent PoraBOND Q capillary column (50 m) with an internal diameter of 0.32 mm and film thickness of 5 μm (part number CP7352). Helium (99.999%) served as the carrier gas with a flow rate of 1.2 ml min through the column. The inlet utilized a glass wool liner and was set to 200 °C. For gas product analysis, 100 μl of gas

was injected into the GCMS using a split injection mode with a 1:1 ratio. Different outlet gas with different cell configurations were collected and tested.

The gas product flux calculation. The total gas product flux calculation was based on the total FE towards CO and H₂ obtained by the GC.

$$\text{Gas product flux (ml/min)} = \frac{i \times t}{e \times F} \times FE_{total} (\%) \times 60 \frac{s}{min} \times 24000 \frac{ml}{mol}$$

Where i is the total current and t is the reaction time, F is the Faraday constant, e is the transferred number for gas product ($e = 2$ for CO and H₂), and FE_{total} is total FE towards CO and H₂ and 24000 ml/mol is the molar gas volume.

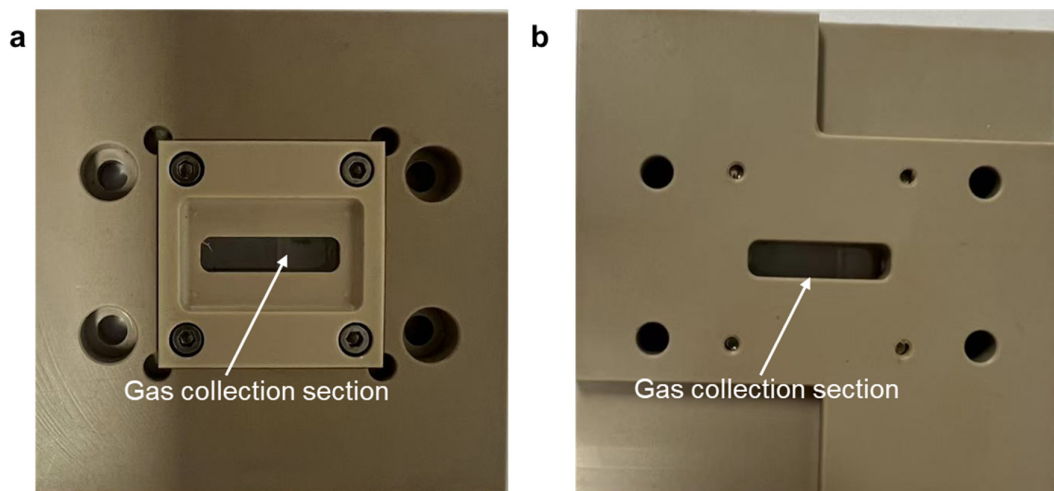


Fig. S1. Photograph of the (a) outside of the gas collection section and (b) inside of the gas collection section.

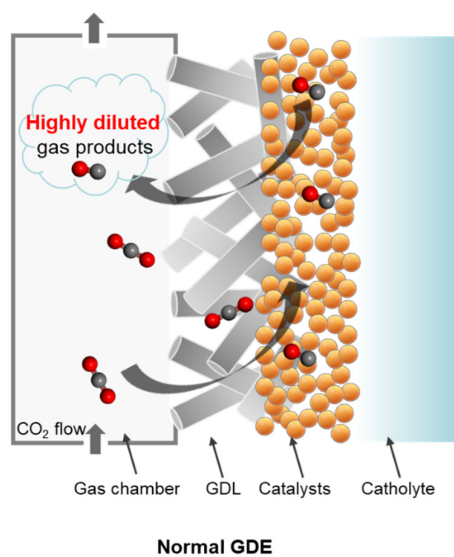


Fig. S2. Schematic of a gas diffusion electrode operated in the ‘normal’ mode. CO₂ flows through the gas chamber and diffuses across the gas diffusion layer to be converted at the catalyst. Any generated gas products quickly mix with the CO₂ reactant, resulting in a dilute output stream.

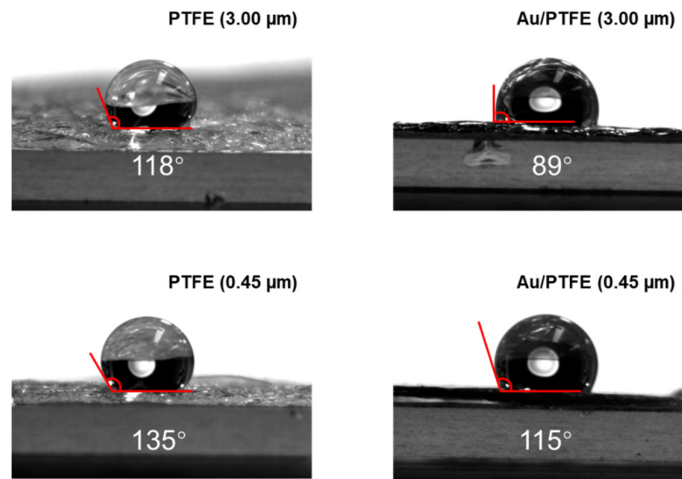


Fig. S3. Contact angle of: (a) PTFE with a pore size of 3 μm , (b) PTFE (3 μm) with 300 nm of Au, (c) PTFE with a pore size of 0.45 μm and (d) PTFE (0.45 μm) with 300 nm of Au.

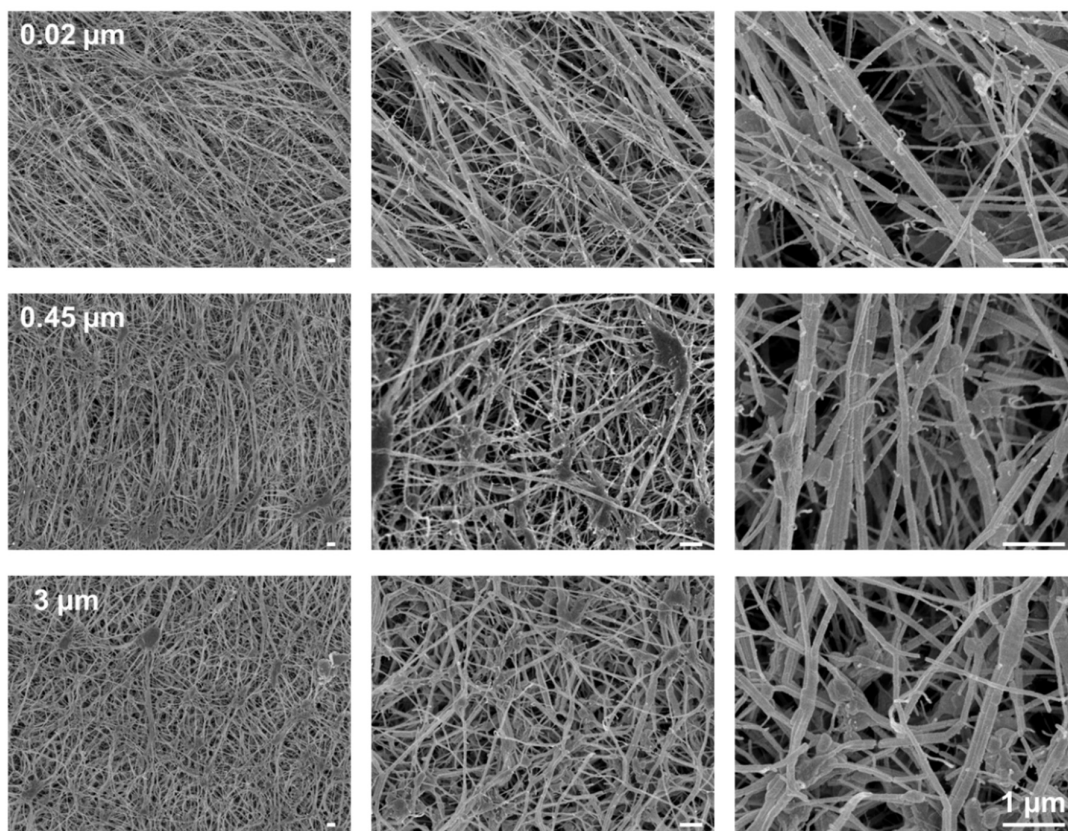


Fig. S4. SEM images of pristine PTFE with different pore sizes. Top row: 0.02 μm , middle row: 0.45 μm and bottom row: 3 μm .

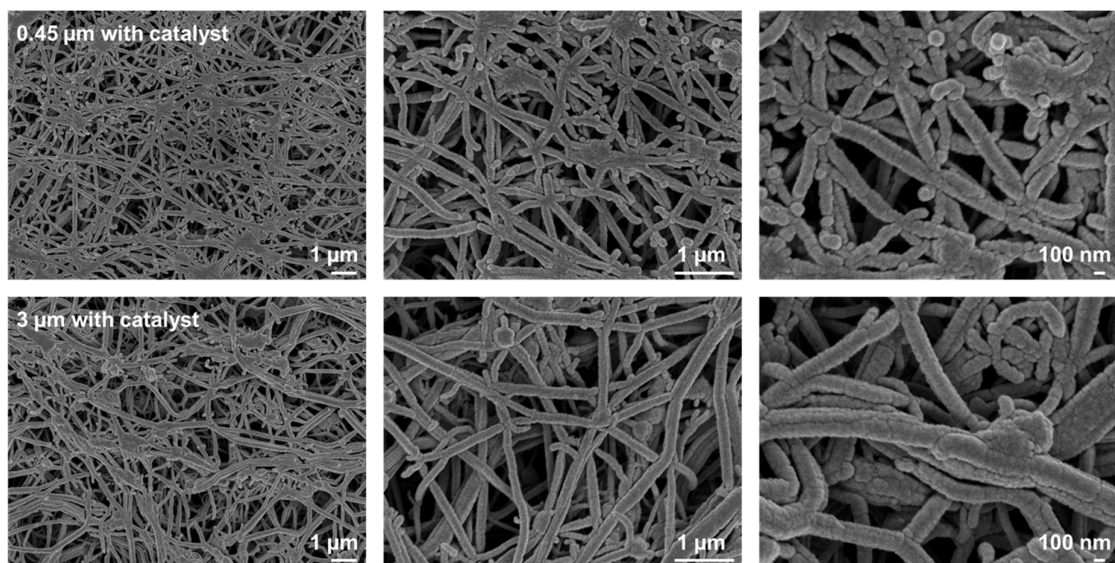


Fig. S5. SEM images of PTFE coated with 300 nm Au by sputtering. Top row: 0.45 μm and bottom row: 3 μm .



Fig. S6. Picture taken at the outlet of the reversed GDE cell under a current density of 80 mA/cm². Continuous output of gas can be observed throughout (Supplementary Video 1).

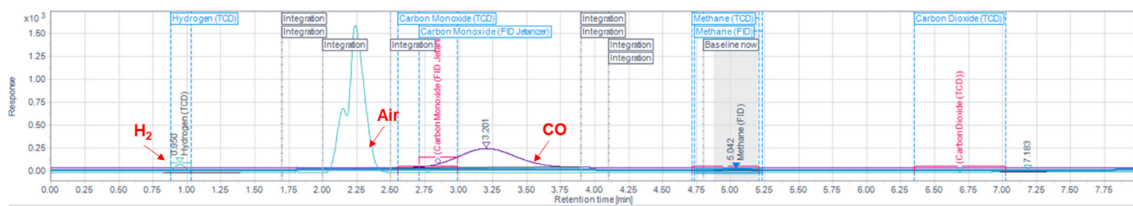


Fig. S7. Screenshot of the gas chromatography of outlet gas obtained from the reversed GDE configuration without any carrier gas. The sample was injected into the GC.

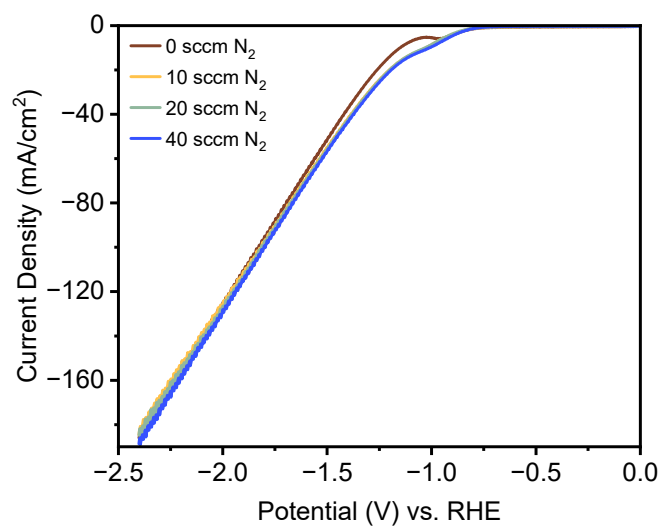


Fig. S8. Linear sweep voltammetry curves of the CO₂R with a different flow rate of the N₂ at the back side of the GDE.

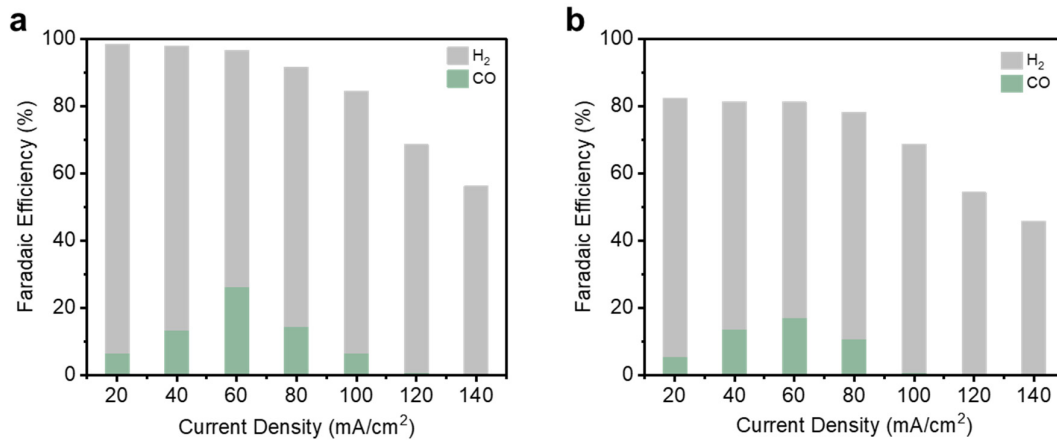


Fig. S9. Product FE for reversed GDE operation mode under a range of different current densities with: (a) Au/PTFE(0.45) and (b) Au/PTFE(3.0). The electrolyte used was CO₂ saturated 1.0 M KHCO₃ electrolyte.

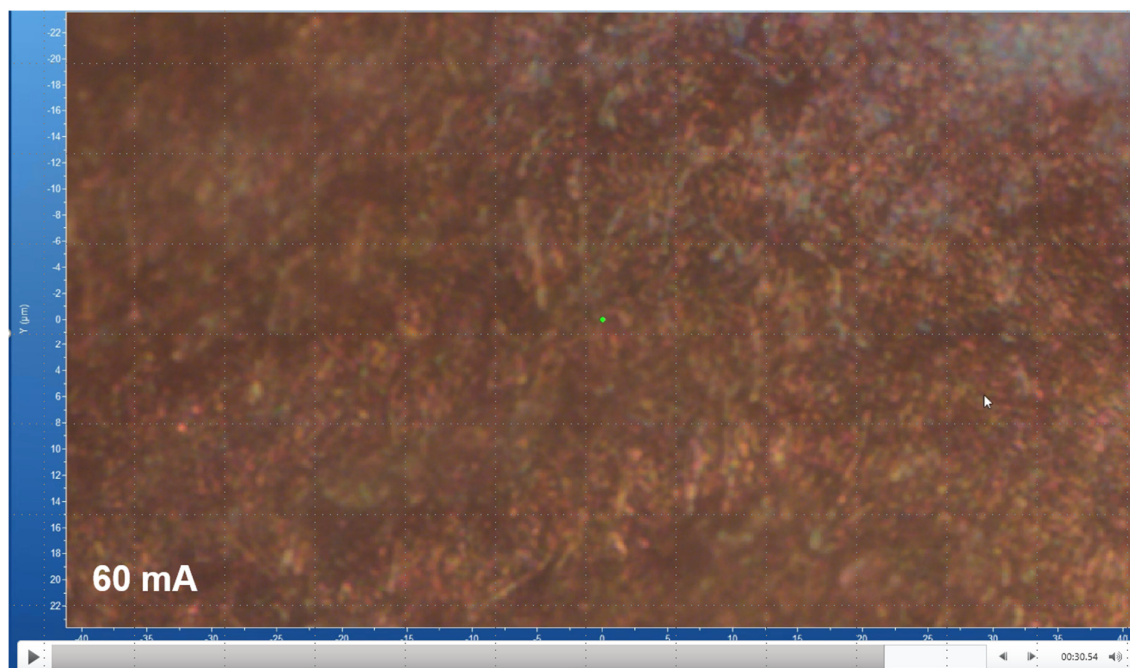


Fig. S10. Screenshot of the gas growth at a current density of 60 mA/cm^2 . No bubble was observed for this condition.



Fig. S11. Screenshot of the gas growth at a current density of 100 mA/cm^2 . We could see two adjacent bubbles, which had been pointed by the red cycles.

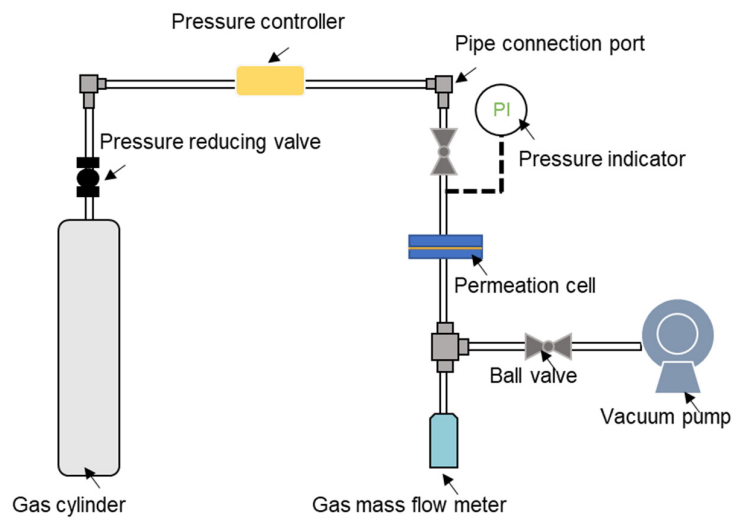


Fig. S12. Schematic illustrations of set up for the gas permeability testing. All models in this schematic are not to scale.

Supplementary Note 1

Determination of Knudsen number and pore flooding.

In Table S1, for each of the GDL pore sizes we list the computed Knudsen number, observed permeance from dry gas permeation experiments, observed permeance from CO₂R experiments, permeance with pore blockage only and pore flooding percentage.

Note that pore flooding is assumed to occur only for the 1 and 3 μm pore sizes in CO₂R experiments. Pore blockage occurs for all pore sizes. For 0.02, 0.1 and 0.45 μm pore sizes, only pore blockage occurs (no pore flooding), hence the permeance with pore blockage only is equal to the observed permeance.

The observed permeances were calculated using the equation below:

$$k = \frac{Q}{A \times \Delta P}$$

Where k is the permrance (GPU), Q is the gas flow through the GDE (m³/s), A is the GDE area in cm², and ΔP is the pressure differential across the GDE (Pa).

The gas permeance with pore blockage only is calculated using the equation below:

$$k_b = k_{CO_2R} \times \frac{k_{dry}}{1.3 \times 10^6}$$

Where k_b is the permeance with pore blockage only (GPU), k_{CO_2R} is observed permeance in CO₂R experiments (GPU), k_{dry} is the observed dry gas permeance (GPU).

The Knudsen number (Kn) is a dimensionless number defined as the ratio of the molecular mean free path length to a representative physical length scale.

$$K_n = \frac{\lambda}{L}$$

Where λ is the mean free path and L is the representative physical length scale. When $Kn > 10$, the flow is Knudsen diffusion. When $0.1 < Kn < 10$, the flow is a type of flow between molecular diffusion and bulk convection. When $0.01 < Kn < 0.1$, the flow is bulk convection.

The observed gas permeance through the GDE in CO₂R experiments is lower than dry gas permeance, which we attribute to be due to pore blockage and flooding of pores. We assume that pore flooding occurs only for GDE with pore sizes of 1 μm and 3 μm . Assuming that the extent of pore blockage observed in 0.02 μm , 0.1 μm , and 0.45 μm remains the same for 1 μm and 3 μm pores, we estimate the permeance reduction due to pore flooding for 1 μm and 3 μm in CO₂R experiments as follows.

Percentage of reduction in permeance due to flooding (%) =

$$100\% \times \left(1 - \frac{\text{Observed permeance in CO}_2\text{R experiment}}{\text{Estimated permeance for dry gas with pore blockage only}} \right)$$

Table S1 Knudsen number and GDE gas permeance values (CO₂R experiments at 120 mA/cm² and pressure gap of 218 Pa as reported in Fig 2b).

Pore size (d) [μm]	Knudsen number (Kn)	Observed permeance (dry gas) [GPU]	Observed permeance (CO ₂ R) [GPU]	Permeance with pore blockage only (CO ₂ R) [GPU]	Pore flooding percentage
0.02	5.19	1.24E+06	6.1E+04		Nil
0.1	1.04	1.27E+06	6.1E+04		
0.45	0.23	1.3E+06	6.1E+04		
1	0.1	1.6E+06	5.8E+04	7.3E+04 (Estimated)	20.5%
3	0.03	3.0E+06	5.2E+04	1.4E+05 (Estimated)	62.9%

Supplementary Note 2

Pressure gap calculations. The pressure gap between the electrolyte and the gas collection chamber was experimentally controlled by adjusting the electrolyte flow rate. To calculate this pressure gap, we modeled our experimental configuration of Fig. S1 in a commercial process simulator called Aspen HYSYS v14. The Beggs & Brill correlation² was used inside Hysys to compute the pressures at various points in the electrolyte and gas collection chamber [A-B] as shown in Fig. S12. This correlation considers the effects of elevation, acceleration, and friction losses on pressure.

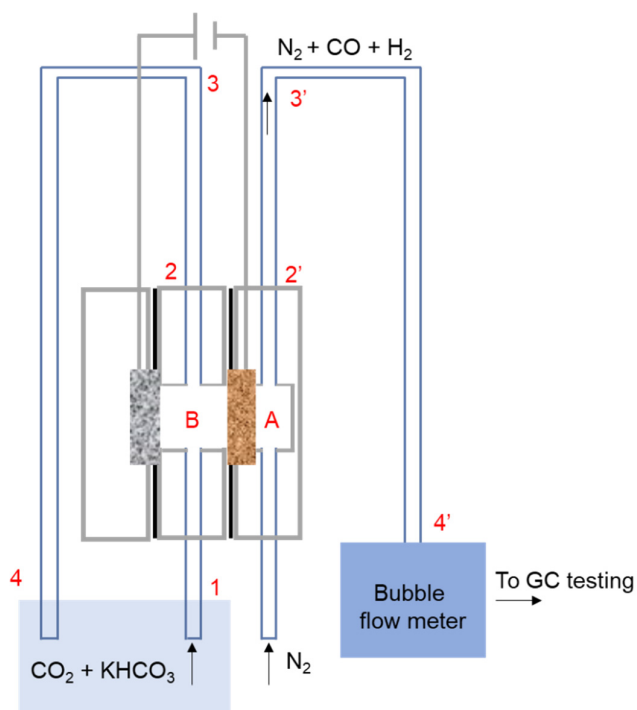


Fig. S13. Schematic of the reversed GDE based cell system.

The pressure gaps (ΔP) from A to B for electrolyte flows of 5 mL/min, 100 mL/min and 150 mL/min are 11 Pa, 218 Pa and 328 Pa respectively.

Table S2. Model input parameters required for calculating the pressure gap.

Parameter	Symbol	Value	Unit
Diameter of tube	$d_{1,2}; d_{2,3}; d_{1,3}; d_{3,4}$	0.2	cm
Diameter of tube	$d_{3,4}$	0.4	cm
Length of tube	$L_{1,2}; L_{2,3}; L_{A,3}; L_{3,4}$	2.5	cm
Length of tube	$L_{3,4}$	10	cm
Viscosity of electrolyte	$\mu_{\text{electrolyte}}$	10^{-3}	Pa.s
N ₂ purge flow rate	Q_{N_2}	30	mL/min
Inlet flow rate	Q_{in}	5/100/150	mL/min
Porosity	ε	0.85	-
Gas viscosity	μ_{gas}	1.74×10^{-5}	Pa.s
Pore length	L_{mem}	250	μm
Active area of GDL	A_{active}	1	cm^2
Surface tension coefficient	γ_{lv}	0.0719	N/m
Density of gas	ρ_v	0.0824	kg/m^3
Density of electrolyte	ρ_l	997	kg/m^3
Pore Diameter	d_{pore}	0.45	μm
		3	μm

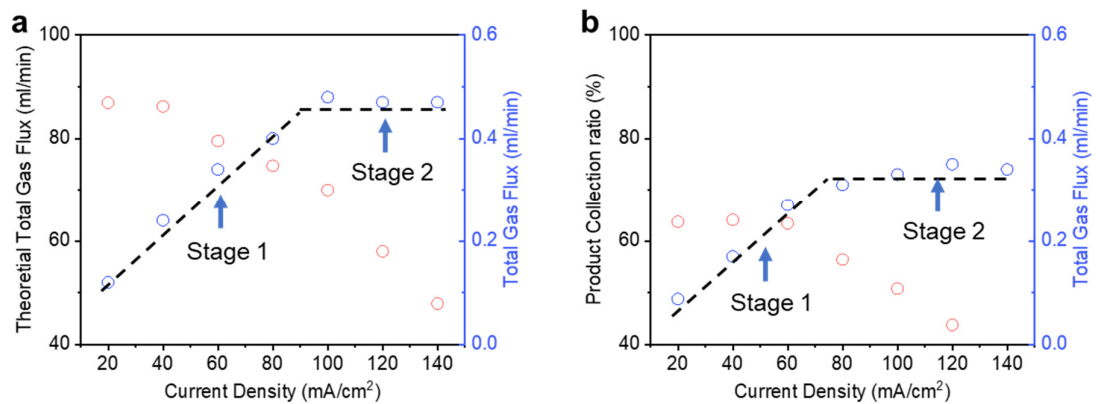


Fig. S14. Product collection ratio and total gas flux at different current density under a pressure gap of 11 Pa with a (a) PTFE with a pore size of 0.45 μm . and (b) PTFE with a pore size of 3.0 μm .

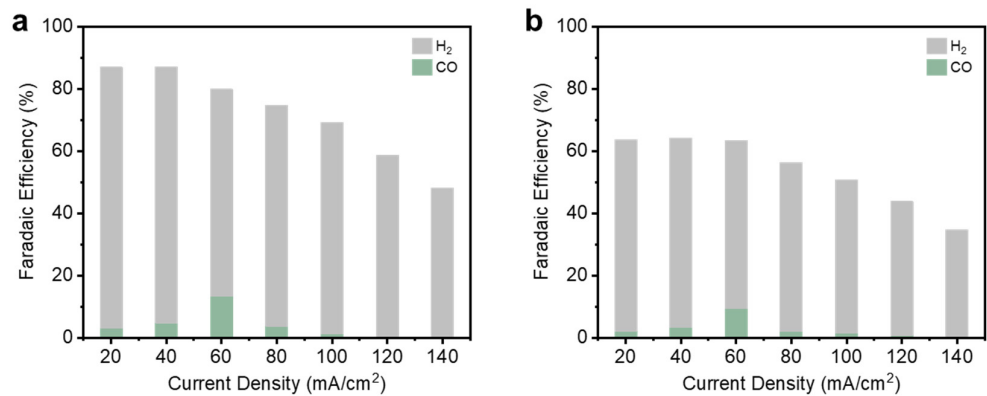


Fig. S15. Product FE for reversed GDE operation mode at various current densities under a pressure gap of 11 Pa with: (a) Au/PTFE(0.45) and (b) Au/PTFE(3.0). The electrolyte used was CO₂ saturated 1.0 M KHCO₃.

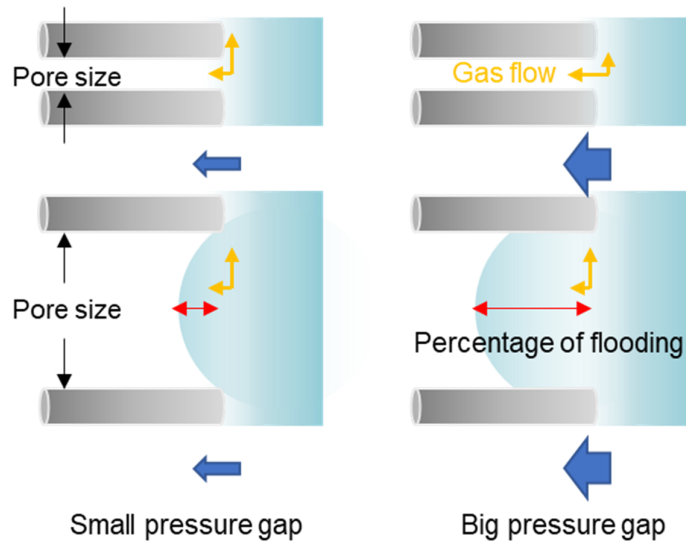


Fig. S16. Schematic of the influence of the pore size and electrolyte pressure on the pore blockage. Top-left: no flooding in small pore with low electrolyte pressure resulting insufficient driving force for gas flow. Top-right: no flooding in small pore with high electrolyte pressure with efficient driving force. Bottom left case: Moderate flooding in large pore size with low electrolyte pressure causing additional resistance for gas transport. Bottom-right case: large pore size with high electrolyte pressure resulting in severe flooding and larger resistance.

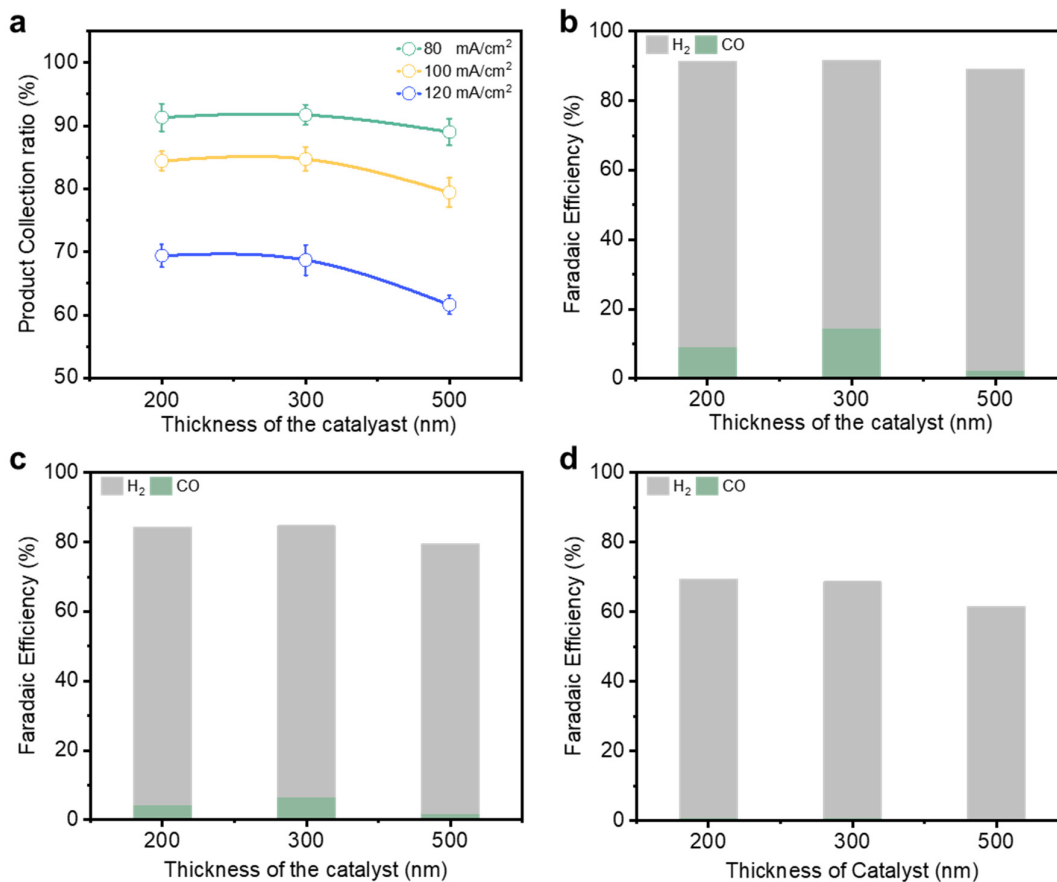


Fig. S17. (a) Gas product collection ratio with different catalyst thickness. CO₂R product FE with different catalyst thickness at a current density of: (b) 80 mA/cm², (c) 100 mA/cm² and (d) 120 mA/cm². All samples used PTFE with a GDL pore size of 0.45 μm.

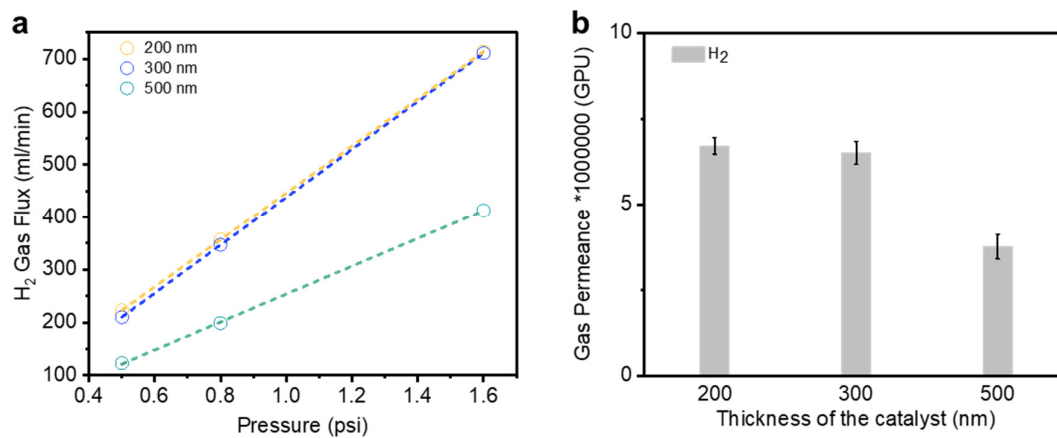


Fig. S18. H₂ gas flux in gas permeation experiments using PTFE with a GDL pore size of 0.45 μm . (b) H₂ gas permeance from gas permeation experiments with different catalyst thickness using PTFE with a GDL pore size of 0.45 μm .

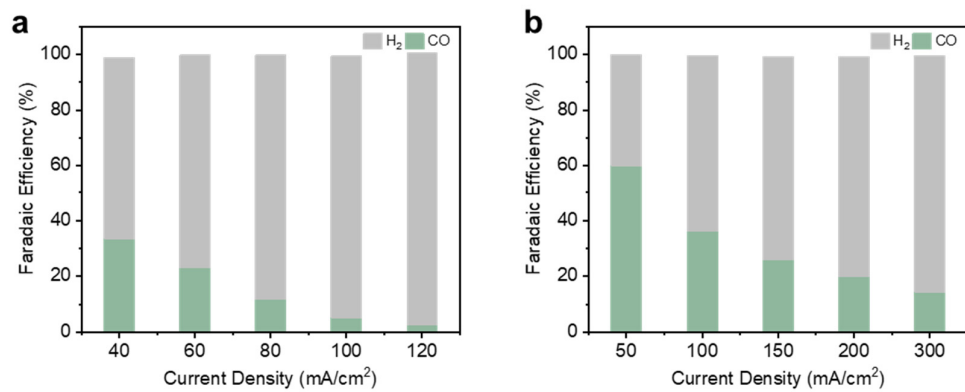


Fig. S19. Product FE with Au/PTFE(0.45) as the cathode in a conventional (a) H-type cell and (b) flow cell system under different current densities using 1.0 M HKCO₃ as the catholyte.

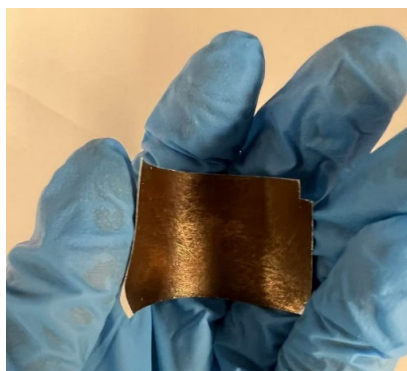


Fig. S20. Photograph of the NP Au/PTFE electrode used in this work.

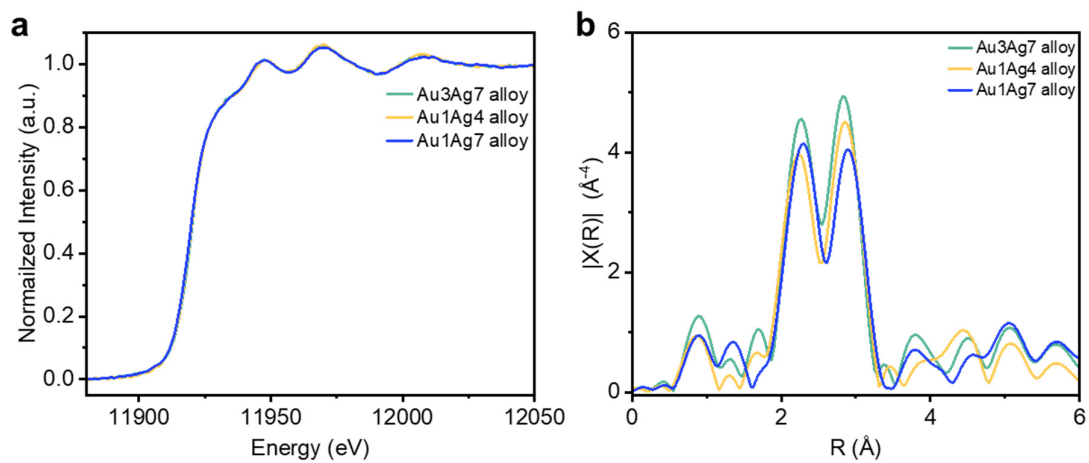


Fig. S21. (a) Au L₃-edge XANES spectra of the different Au-based catalysts. (b) Au L₃-edge Fourier-transformed (FT) k^3 -weighted $\chi(k)$ functions of Au/PTFE.

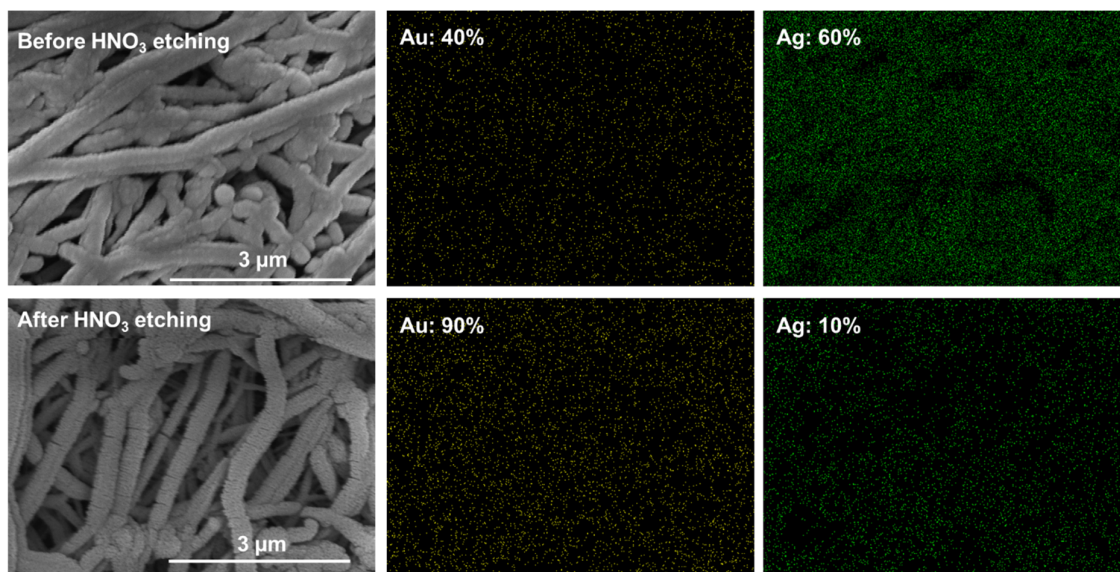


Fig. S22. SEM energy-dispersive spectroscopy (EDS) mapping of Au based catalyst before and after KNO_3 etching.

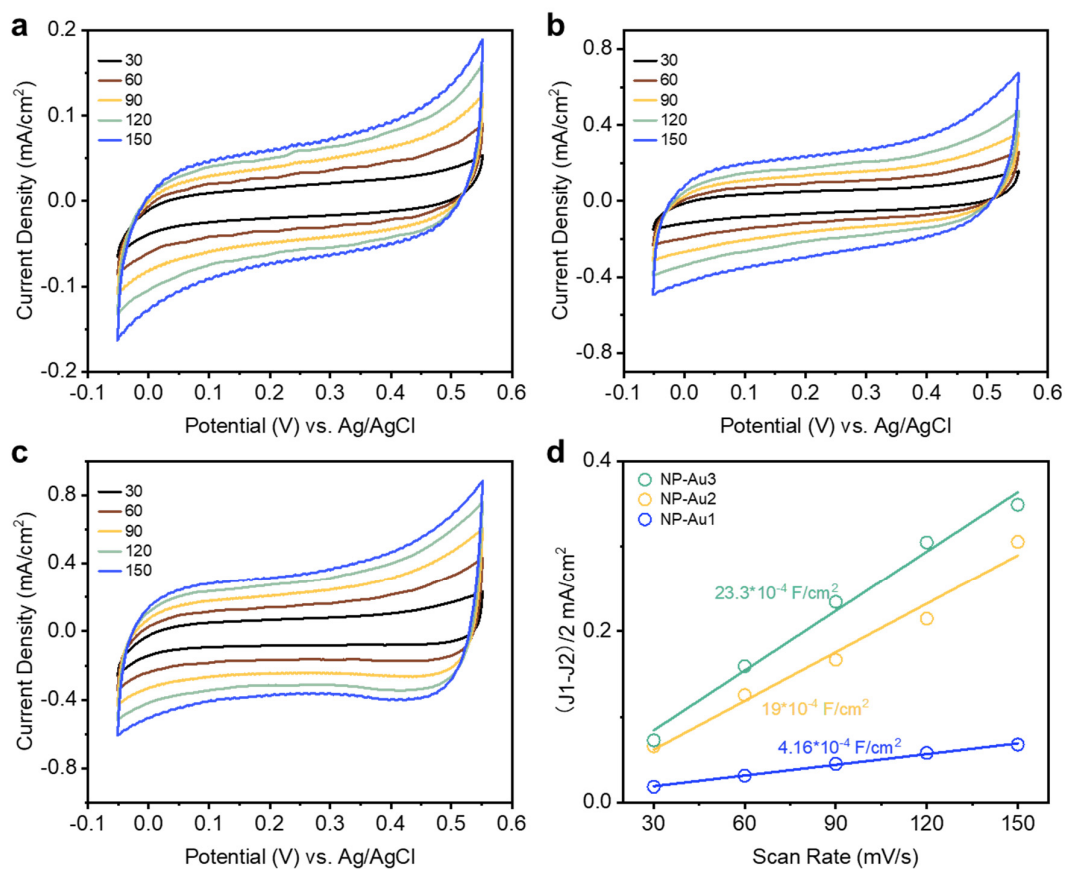


Fig. S23. Effective electrochemical active surface area tests (ECSA) of (a) NP-Au1. (b) NP-Au2, and (c) NP-Au3. (d) Electrochemical double-layer capacity of NP-Au1, NP-Au2, and NP-Au3. NP-Au1 represents the nanoporous Au from a Au₁Ag₇ alloy and NP-Au2 represents the nanoporous Au from a Au₁Ag₄ alloy. NP-Au3 (named nanoporous Au in manuscript) represents the nanoporous Au derived from an Au₃Ag₇ alloy and exhibits the highest double-layer capacity of $23.3 \times 10^{-4} \text{ F/cm}^2$.

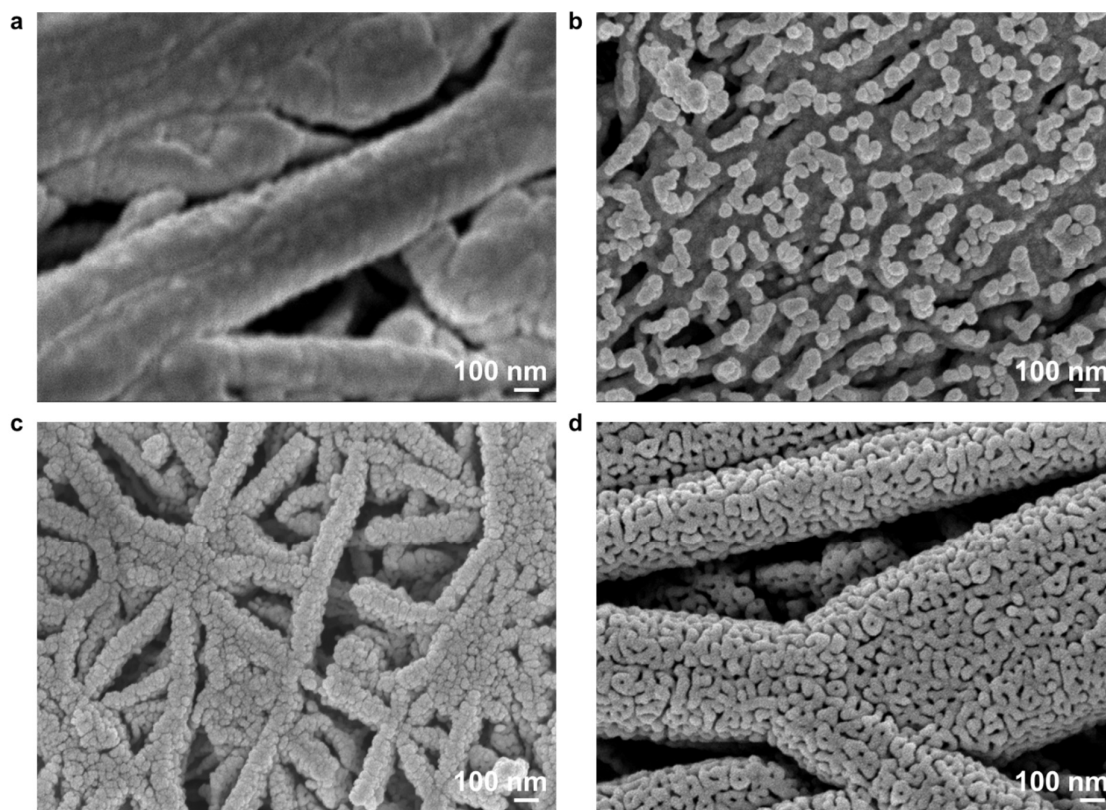


Fig. S24. SEM images of (a) Au. (b) NP-Au1. (c) NP-Au2. and (d) NP-Au3. NP-Au1 represents the nanoporous Au from a Au_1Ag_7 alloy and NP-Au2 represents the nanoporous Au from a Au_1Ag_4 alloy. NP-Au3 (named nanoporous Au in manuscript) represents the nanoporous Au derived from an Au_3Ag_7 alloy.

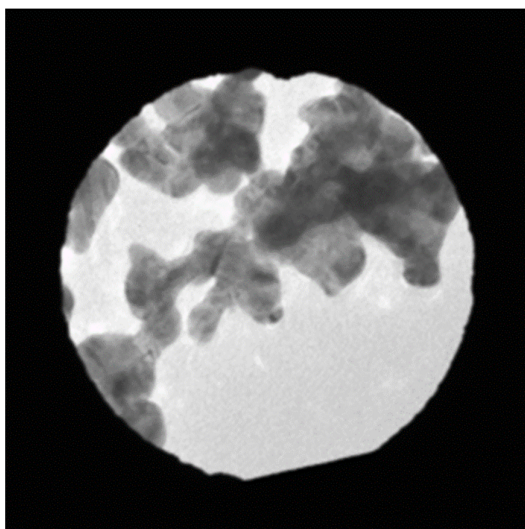


Fig. S25. Selected area aperture for the electron diffraction patterns.

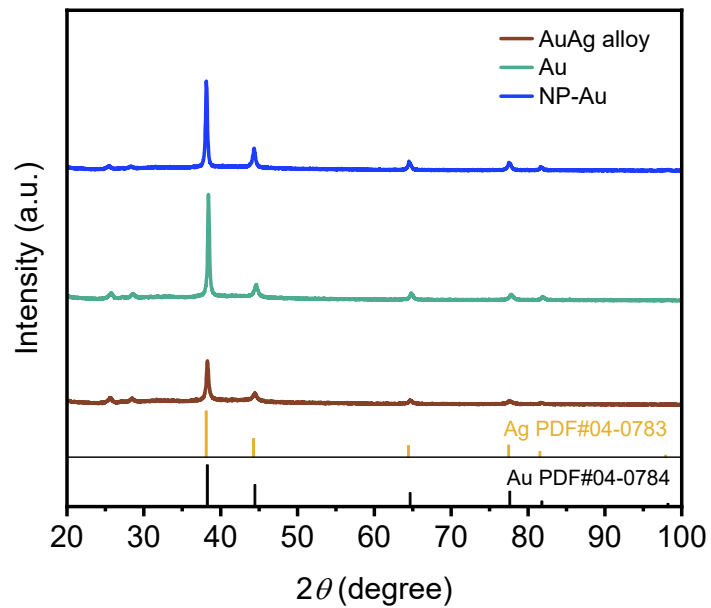


Fig. S26. Powder XRD patterns of NP-Au, Au and AuAg alloy.

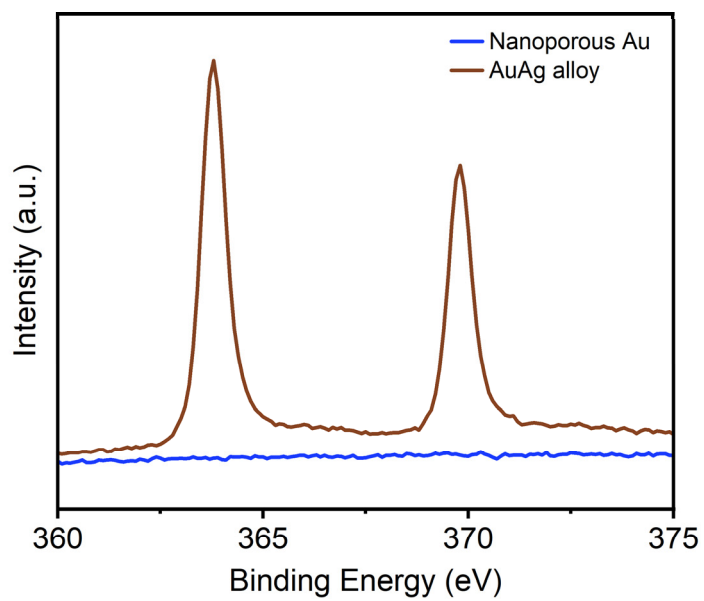


Fig. S27. Ag 3d X-ray photoelectron spectroscopy (XPS) spectra of the different Au based samples.

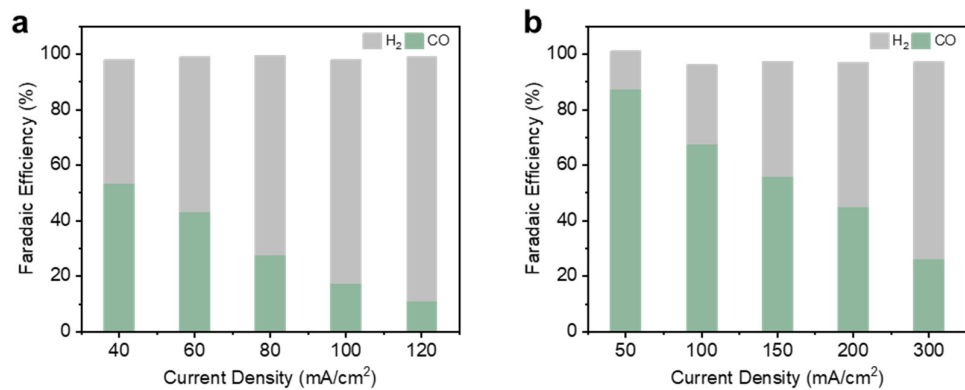


Fig. S28. Product FE with NP Au/PTFE as catalyst in a (a) H-type cell and (b) normal GDL electrode under different current densities using 1.0 M HKCO₃ as the catholyte.

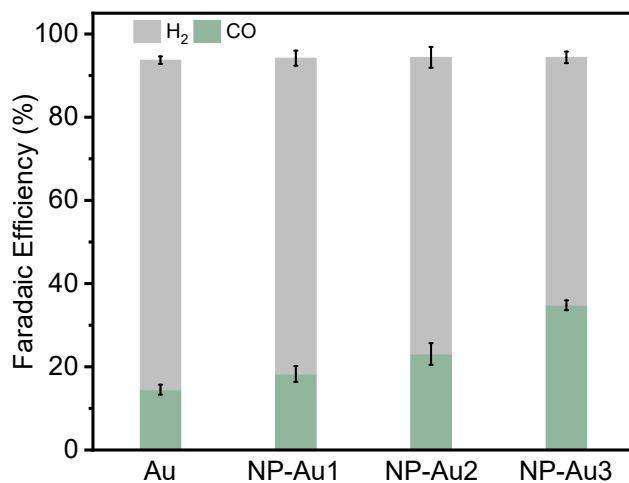


Fig. S29. CO₂R product FE for the different Au-based catalysts in the reversed GDL based cell. NP-Au1 represents the nanoporous Au from a Au₁Ag₇ alloy and NP-Au2 represents the nanoporous Au from a Au₁Ag₄ alloy. NP-Au3 represents the nanoporous Au derived from an Au₃Ag₇ alloy (denoted as nanoporous Au in the manuscript) and exhibits the highest FE to CO at 34.8%. All data collected at this figure were obtained at 80 mA/cm².

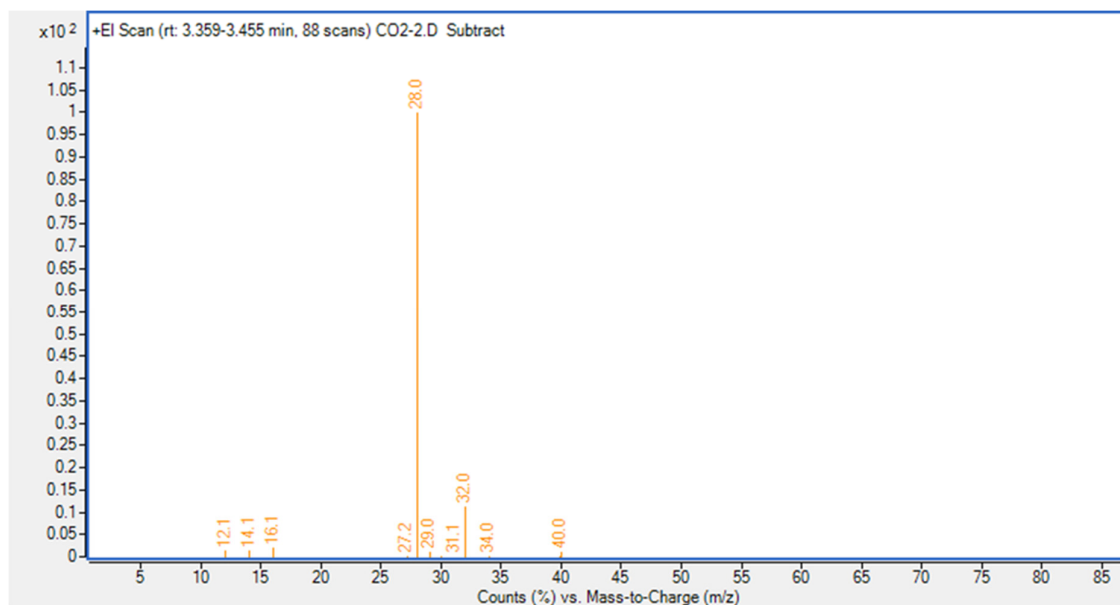


Fig. S30. Screenshot of the mass spectrum of our sample from the peak at around 3.4 min from GCMS analysis. This peak is assigned to CO.

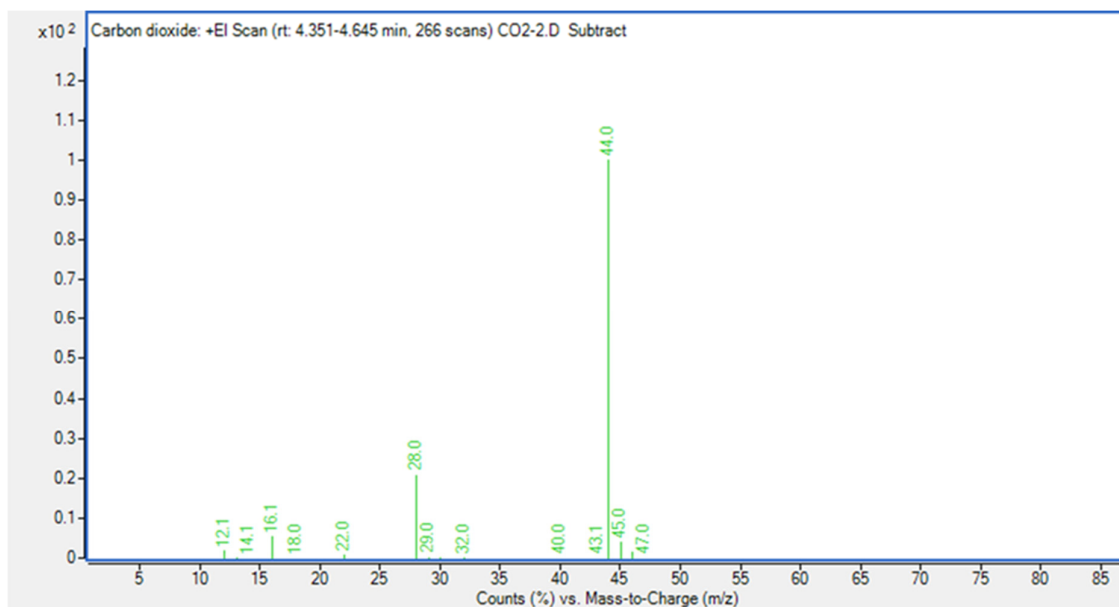


Fig. S31. Screenshot of the mass spectrum of our sample from the peak at around 4.5 min from GCMS analysis. This peak is assigned to CO₂.

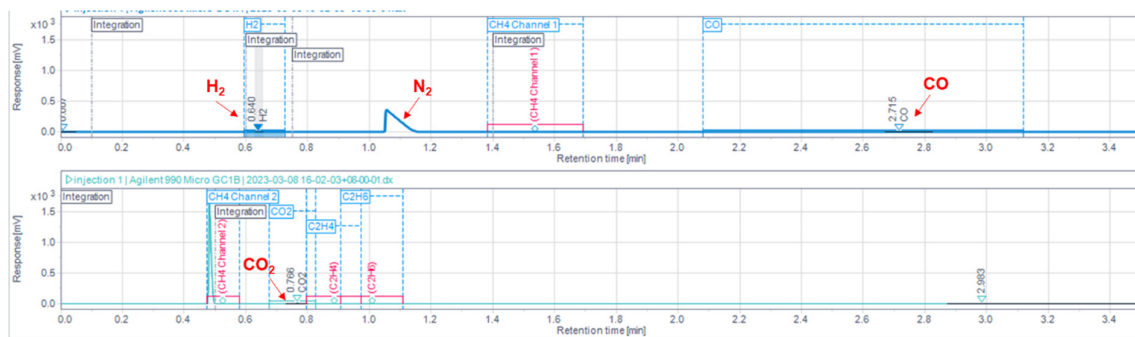


Fig. S32. Screenshot of the GC spectrum of the outlet gas obtained from the reversed GDL configuration with a cofeeding of CO₂ (95%) and O₂ (5%). As shown in the screenshot, no CO₂ or O₂ was observed.

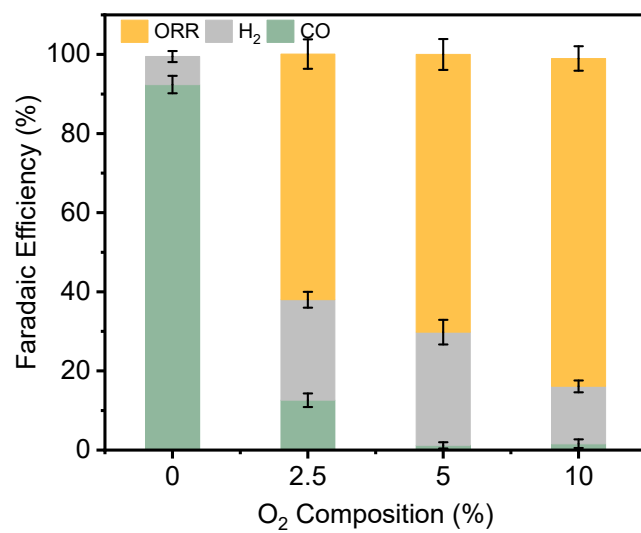


Fig. S33. CO₂R product FE obtained with different O₂ impurity compositions for normal GDL (flow cell). In all cases, a constant current density of 80 mA/cm² was applied.

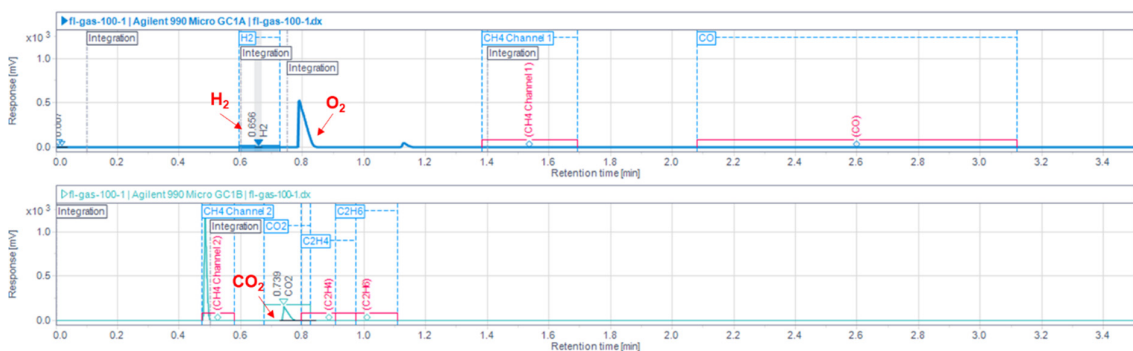


Fig. S34. Screenshot of the GC spectrum of outlet gas obtained from the normal GDL (flow cell) configuration with cofeeding of CO₂ (95%) and O₂ (5%). As shown in the screenshot, no CO was observed.

Table S3. Faradaic efficiency of products obtained in Au/PTFE(0.45) under a pressure gap of 218 Pa.

Current density (mA/cm ²)	H ₂ FE (%)	CO FE (%)
20	91.9	6.7
40	84.7	13.4
60	70.4	26.3
80	77.2	14.5
100	78.1	6.6
120	67.9	0.8
140	56.1	0.2

Table S4. Faradaic efficiency of products obtained in Au/PTFE(3.00) under a pressure gap of 218 Pa.

Current density (mA/cm ²)	H ₂ FE (%)	CO FE (%)
20	77	5.6
40	67.8	13.7
60	64	17.3
80	67.4	10.9
100	68.1	0.8
120	53.9	0.6
140	45.9	0.1

Table S5. Faradaic efficiency of products obtained in Au/PTFE(0.45) under a pressure gap of 11 Pa.

Current density (mA/cm ²)	H ₂ FE (%)	CO FE (%)
20	83.7	3.2
40	82.1	4.9
60	66.3	13.5
80	70.9	3.8
100	67.8	1.3
120	58.1	0.6
140	47.9	0.3

Table S6. Faradaic efficiency of products obtained in Au/PTFE(3.00) under a pressure gap of 11 Pa.

Current density (mA/cm ²)	H ₂ FE (%)	CO FE (%)
20	61.4	2.3
40	60.6	3.5
60	53.9	9.5
80	54.3	2.1
100	49.2	1.6
120	42.9	0.9
140	34.3	0.4

Table S7. Faradaic efficiency of products obtained in PTFE(0.45) with different thickness of catalyst under a pressure gap of 218 Pa at different current density.

Current density (mA/cm ²) Thickness of the catalyst (nm)	H ₂ FE (%)	CO FE (%)
80 mA/cm ² (200 nm)	82.2	9.1
80 mA/cm ² (300 nm)	77.2	14.5
80 mA/cm ² (500 nm)	86.7	2.3
100 mA/cm ² (200 nm)	80.1	4.3
100 mA/cm ² (300 nm)	78.1	6.6
100 mA/cm ² (500 nm)	77.5	1.9
120 mA/cm ² (200 nm)	68.5	0.9
120 mA/cm ² (300 nm)	67.9	0.8
120 mA/cm ² (500 nm)	61.3	0.3

Table S8. Faradaic efficiency of products obtained in nanoporous Au/PTFE(0.45) under a pressure gap of 218 Pa.

Current density (mA/cm ²)	H ₂ FE (%)	CO FE (%)
20	73.6	24.5
40	60.7	38.4
60	50.2	46.7
80	57.3	34.8
100	73.1	12.7
120	67.4	3.9

Supplementary Video 1. Continuous outflow of gas product from the collection chamber.

Supplementary Video 2. Monitoring the catalyst surface using an immersion optical microscope at a current density of 60 mA/cm².

Supplementary Video 3. Monitoring the catalyst surface using an immersion optical microscope at a current density of 100 mA/cm².

References

- 1 Fenwick, A. Q. *et al.* Probing the catalytically active region in a nanoporous gold gas diffusion electrode for highly selective carbon dioxide reduction. *ACS Energy Letters* 7, 871-879 (2022).
- 2 Venkateswar, R. *A method to calculate pressure drop for gas-liquid flow in long horizontal transmission lines.* (Oklahoma State University, 1987).